2

Simulation of the Scavenging Process in Two-Stroke Engines

María Isabel Lamas Galdo and Carlos G. Rodríguez Vidal
Universidade da Coruña
Spain

1. Introduction

It is widely known that the scavenging process plays a very important role in the performance and efficiency of two-stroke engines. Briefly, scavenging is the process by which the fresh charge displaces the burnt gas from the cylinder. Due to the difficulties associated with the measurement techniques, CFD (Computational Fluid Dynamics) is a very helpful tool to analyze the flow pattern inside the cylinder. CFD simulations can provide more detailed information than experimental studies. For this reason, this chapter focuses on a numerical analysis to simulate the fluid flow and heat transfer inside the cylinder at the scavenging process.

This chapter is a continuation and extension of previous works (Lamas-Galdo *et al.,* 2011; Lamas & Rodriguez, 2012), in which CFD models were developed and validated with experimental results. The content is organized as follows. A brief description of two-stroke engines is given in Section 2. The mathematical model, i.e., the governing equations are presented in Section 3 and the numerical model is discussed in Section 4. After that, the results are shown in Section 5 and the conclusions of this chapter are discussed in Section 6.

2. Introduction to the two-stroke engine

Although the focus of this chapter is the numerical treatment of the scavenging process, it is important to introduce certain introductory aspects about the performance of two-stroke engines. This will facilitate the reader's understanding of the chapter.

2.1 Mechanical aspects

A two-stroke engine is an internal combustion engine that completes the process cycle in one revolution of the crankshaft or two strokes of the piston: an up stroke and a down stroke. Both spark ignition and compression ignition engines exist today. Spark ignition engines are employed in light applications (chainsaws, motorcycles, outboard motors, etc) due to its low cost and simplicity. On the other hand, diesel compression ignition engines are mainly employed in large and weight applications, such as large industrial and marine engines, heavy machinery, locomotives, etc. Fig. 1 (a) shows a spark ignition engine installed on a motorbike and Fig. 1 (b) shows a large compression ignition engine, the MAN B&W 7S50MC, typically used in marine propulsion and industrial plants.

(a) (b)

Fig. 1. (a) Spark ignition gasoline engine installed on a motorcycle. (b) Compression ignition diesel engine MAN B&W 7S50MC installed on a ship.

There are several mechanical details which vary from one engine to another. For example, Fig. 2 (a) shows a cross section of the spark ignition engine shown in Fig. 1 (a). In this engine, the charge is introduced to the cylinder by ports. The opening and closing of the ports is controlled by the sides of the piston covering and uncovering them as it moves up and down in the cylinder. As can be seen in the bottom part of Fig. 2 (a), this engine has a crankcase. This is a separate charging cylinder which employs the volume below the piston as a charging pump. On the other hand, Fig. 2 (b) shows a cross section of the compression ignition engine illustrated on Fig. 1 (a). This engine has one exhaust valve and several intake ports. In this case, the external air is introduced directly in the cylinder instead of being pumped from the crankcase.

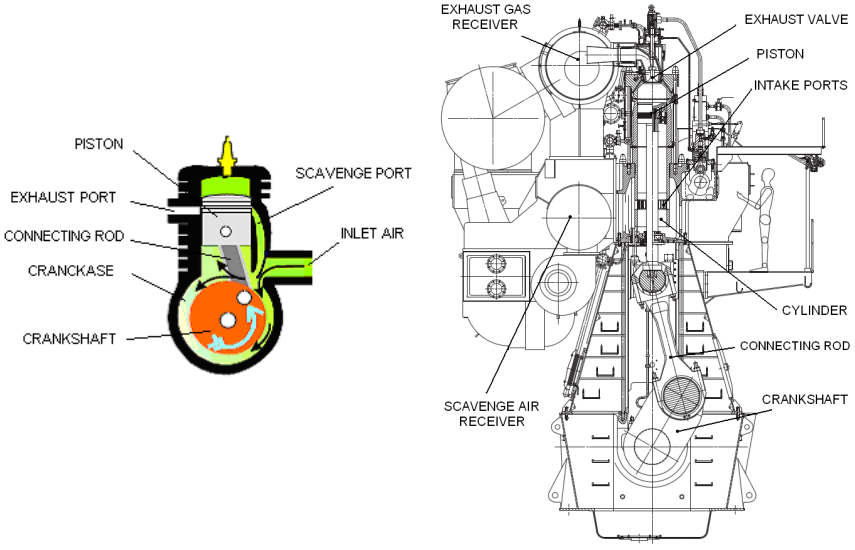

(a) (b)

Fig. 2. (a) Cross section of a spark ignition engine. (b) Cross section of a compression ignition engine, the MAN B&W 7S50MC.

2.2 The scavenging process

Before discussing the scavenging process, it is useful to describe the operation cycle of the two-stroke engine with direct injection. For this purpose, an engine with scavenge and exhaust ports instead valves will be considered. At the beginning of the cycle, when fuel injection and ignition have just taken place, the piston is at the TDC (top dead center). The temperature and pressure rise and consequently the piston is driven down, Fig. 3 (a) (note that the arrows indicate the direction of the piston). Along the power stroke, the exhaust ports are uncovered (opened) and, consequently, the burnt gases begin to flow out, Fig. 3 (b). The piston continues down. When the piston pasts over (and consequently opens) the scavenge ports, pressurized air enters and drives out the remaining exhaust gases, Fig. 3 (c). This process of introducing air and expelling burnt gases is called scavenging. The incoming air is used to clean out or scavenge the exhaust gases and then to fill or charge the space with fresh air. After reaching BDC (bottom dead center), the piston moves upward on its return stroke. The scavenge ports and then the exhaust ports are closed, Fig. 3 (d), and the air is then compressed as the piston moves to the top of its stroke. Soon before the piston reaches TDC, the injectors spray the fuel, the spark plug ignite the mixture and the cycle starts again.

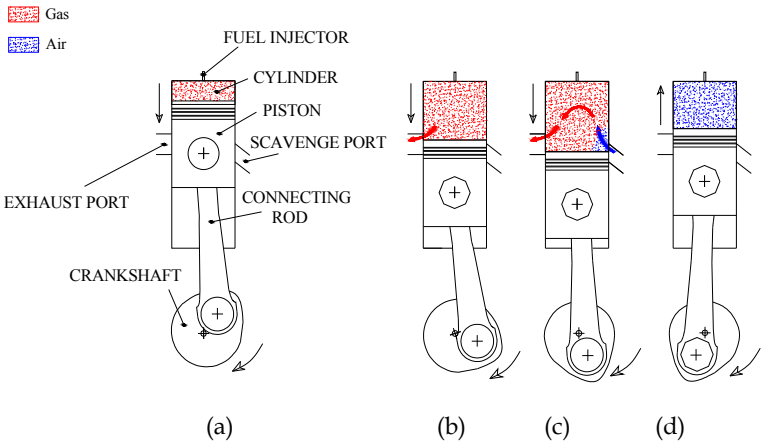

Fig. 3. Basic engine operation. (a) Injection; (b) exhaust; (c) scavenge; (d) compression.

A drawback which has a decisive influence, not only on consumption but also on power and pollution, is the process of displacing the burnt gases from the cylinder and replacing them by the fresh-air charge, known as scavenging. In ideal scavenging, the entering scavenge air acts as a wedge in pushing the burnt gases out of the cylinder without mixing with them. Unfortunately, the real scavenging process is characterized by two problems common to two-stroke engines in general: *short-circuiting losses* and *mixing*. *Short-circuiting* consists on expelling some of the fresh-air charge directly to the exhaust and *mixing* consists on the fact

that there is a small amount of residual gases which remain trapped without being expelled, being mixed with some of the new air charge.

The main difficulty involved in designing an effective scavenging system is that there are too involving variables: piston chamber geometry, intake and exhaust ports design, opening and closing timings, compression ratio, fuel composition, inlet and exhaust pressures, etc, being necessary a detailed study to embrace all this factors. For years, the study of the fluid flow inside engines has been mainly supported by experimental tests such as PIV (Particle Image Velocity), LDA (Laser Doppler Anemometry), ICCD cameras, etc. However, these experimental tests are very laborious and expensive. As an alternative solution to experimental techniques, CFD has recently become a useful tool to study the fluid flow inside engines. In the field of engines, CFD is especially useful to design complex components such as combustion chambers, manifolds, injectors and other parameters. The first numerical simulations of engines appeared in the eighties (Sher, 1980; Carpenter & Ramos, 1986; Sweeny *et al.*, 1985; Ahmadi-Befrui *et al.*, 1989) but, unfortunately, these first numerical studies only provided, with poor accuracy, information about the general configuration of the flow field inside the cylinder. Besides, at that time it was very difficult to carry out a three-dimensional analysis. After these first numerical studies, a lot of works appeared in the nineties and in recent years. The number of CFD codes has also increased noticeably, appearing studies using KIVA (Epstein *et al.*, 1991; Amsden *et al.*, 1992), STAR-CD (Raghunathan & Kenny, 1997; Yu *et al.* 1997; Zahn *et al.*, 2000; Hariharan *et al.*, 2009), FIRE (Hori *et al.*, 1995; Laimböck *et al.*, 1998) Fluent (Pitta & Kuderu, 2008; Lamas-Galdo *et al.*, 2011), CFX (Albanesi *et al.*, 2009), etc.

3. Mathematical model

Once the basic performance of two-stroke engines was described, the methodology to simulate the scavenging process will be treated in this section.

3.1 Governing equations

The governing equations of the flow inside the cylinder are the Navier-Stokes ones. The energy equation is also needed to compute the thermal problem. Finally, as there are two components (air and burnt gases), one more equation must be added to characterize the propagating interface. These equations are briefly described in what follows.

In Cartesian tensor form, the continuity equation is given by:

$$\frac{\partial \rho}{\partial t} + \frac{\partial}{\partial x_i}\left(\rho u_i\right) = 0 \tag{1}$$

where ρ is the density and u the velocity. It is very common to consider the flows as ideal gasses, so the density can be calculated as follows:

$$\rho = \frac{p}{RT} \tag{2}$$

where p is the pressure, T the temperature and R the ideal gas constant. The momentum conservation equation is given by:

$$\frac{\partial}{\partial t}(\rho u_i) + \frac{\partial}{\partial x_j}(\rho u_i u_j) = -\frac{\partial p}{\partial x_i} + \frac{\partial \tau_{ij}}{\partial x_j} \tag{3}$$

where τ_{ij} is the stress tensor. If the fluid is treated as Newtonian, the stress tensor components are given by:

$$\tau_{ij} = \mu\left(\frac{\partial u_i}{\partial x_j} + \frac{\partial u_j}{\partial x_i} - \frac{2}{3}\delta_{ij}\frac{\partial u_k}{\partial x_k}\right) \tag{4}$$

As only the scavenging process and not the combustion is treated on this chapter, only two components need to be computed: burnt gas and unburnt gas (air). In order to characterize the propagating interface, the following equation is solved:

$$\frac{\partial(\rho Y_{air})}{\partial t} + \nabla \cdot (Y_{air}\rho\vec{V}) = 0 \tag{5}$$

where Y_{air} is the mass fraction of the air. The mass fraction of the burnt gases, Y_{gas} , is given by the restriction that the total mass fraction must sum to unity:

$$Y_{gas} = 1 - Y_{air} \tag{6}$$

3.2 Turbulence

Today's standard in engine simulation are Reynolds Averaged Navier-Stokes (RANS) methods. Another approach are Large Eddy Simulation (LES) techniques. LES and RANS techniques differ in the way they address the present impossibility to resolve all the scales present in engine flows. RANS simulations are based on a statistical averaging to solve only the mean flow. This implies that modelling concerns the whole spectrum of scales. In LES, a spatial or temporal filtering is used to represent the large turbulent scales of the flow, which are directly resolved, while the small scales are modeled. In LES, modeling thus concerns a much smaller part of the spectrum, which leads to an improvement of predictivity as compared to RANS. LES inherently allows to address large scale unsteady phenomena, and thus has a good potential to predict engine unsteadiness. The problem is that LES would lead to a CPU time that is way beyond reach of present supercomputers. Therefore, the use o LES is not very common.

In the field of RANS methods, the two-equation model standard k-ε is the most used to simulate engines. The RNG k-ε model is also widely employed, specially in the cases of swirling flows.

The momentum conservation equation for a turbulent flow is given by:

$$\frac{\partial}{\partial t}(\rho u_i) + \frac{\partial}{\partial x_j}(\rho u_i u_j) = -\frac{\partial p}{\partial x_i} + \frac{\partial \tau_{ij}}{\partial x_j} + \frac{\partial}{\partial x_j}(-\rho\overline{u_i' u_j'}) \tag{7}$$

A common method to model the Reynolds stresses, $-\rho\overline{u_i' u_j'}$, is the Boussinesq hypothesis to relate the Reynolds stresses to the mean velocity gradients:

$$-\rho\overline{u_i' u_j'} = \mu_t\left(\frac{\partial u_i}{\partial x_j}+\frac{\partial u_j}{\partial x_i}\right)-\frac{2}{3}\left(\rho k+\mu_t\frac{\partial u_k}{\partial x_k}\right)\delta_{ij} \tag{8}$$

where δ_{ij} is the Kronecker delta (δ_{ij}=1 if $i=j$ and δ_{ij}=0 if $i\neq j$), which is included to make the formula applicable to the normal Reynolds stresses for which $i=j$ (Versteeg and Malalasekera, 2007) and μ_t is the turbulent viscosity. The k-ε model includes two differential equations, corresponding to the turbulent kinetic energy (k), and its dissipation rate (ε), given by Ecs. (9) and (10) respectively.

$$\frac{\partial}{\partial t}(\rho k)+\frac{\partial}{\partial x_i}(\rho k u_i)=\frac{\partial}{\partial x_j}\left[\alpha_k\mu_t\frac{\partial k}{\partial x_j}\right]+G_k+G_b-\rho\varepsilon-Y_M \tag{9}$$

$$\frac{\partial}{\partial t}(\rho\varepsilon)+\frac{\partial}{\partial x_i}(\rho\varepsilon u_i)=\frac{\partial}{\partial x_j}\left[\alpha_\varepsilon\mu_t\frac{\partial \varepsilon}{\partial x_j}\right]+C_{1\varepsilon}\frac{\varepsilon}{k}\left(G_k+G_{3\varepsilon}G_b\right)-C_{2\varepsilon}\rho\frac{\varepsilon^2}{k} \tag{10}$$

In the above equations, G_k represents the generation of turbulence kinetic energy due to the mean velocity gradients; G_b is the generation of turbulence kinetic energy due to buoyancy; Y_M represents the contribution of the fluctuating dilatation in compressible turbulence to the overall dissipation rate. C_μ, $C_{1\varepsilon}$, $C_{2\varepsilon}$, $C_{3\varepsilon}$, σ_k and σ_ε are constants and the terms a_k and a_ε represent the inverse effective Prandtl numbers for k and ε respectively. These quantities were obtained by a RNG modified method which accounts for the effects of swirl or rotation. Details of the procedure are given elsewhere, (Fluent Inc., 2006).

The turbulent viscosity, μ_t, is computed by combining k and ε as follows:

$$\mu_t=\rho C_\mu\frac{k^2}{\varepsilon} \tag{11}$$

Concerning the heat transfer problem, turbulent heat transport can be modeled using the concept of Reynolds' analogy to turbulent momentum transfer. The energy equation is thus given by the following:

$$\frac{\partial}{\partial t}(\rho E)+\frac{\partial}{\partial x_i}\left[u_i(\rho E+p)\right]=\frac{\partial}{\partial x_j}\left[\left(k_t+\frac{C_p\mu_t}{\mathrm{Pr}}\right)\frac{\partial T}{\partial x_j}+u_i\tau_{ij}\right] \tag{12}$$

where E is the total energy.

4. Numerical procedure

In this section, the generation of the mesh and other numerical details will be described. Particularly, this section focuses on the engine studied in Lamas-Galdo *et al.* (2011), which is shown in Fig. 1 (a) and Fig. 2 (a). This is a single cylinder two-stroke engine. The geometry and distribution diagram are shown in Fig. 4, and other technical specifications are summarized in Table 1.

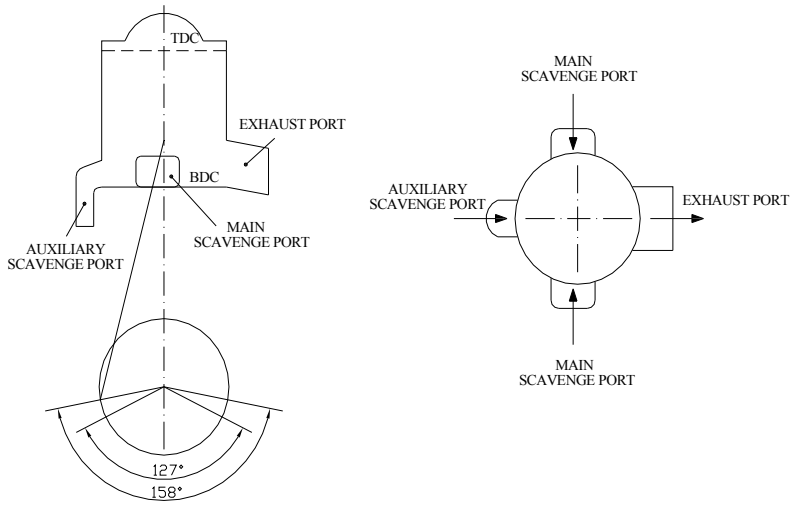

(a) (b)

Fig. 4. Cylinder geometry and distribution diagram. (a) Lateral view; (b) Plant view. Lamas-Galdo *et al.* (2011).

Parameter	Value
Type of engine	Two-stroke, Otto
Displacement (cm^3)	127.3
Compression rate	9.86:1
Bore (mm)	53.8
Stroke (mm)	56
Connecting rod length (mm)	110
Scavenging system	Loop scavenge
Fuel system	Direct injection
Power (W)	7500
Speed (rpm)	6000

Table 1. Technical specifications.

At maximum continuum rating, the in-cylinder, exhaust and intake pressures were measured experimentally. Piezoresistive sensors were employed to measure the exhaust and intake pressures, while a piezoelectric sensor was employed to measure the in-cylinder pressure. These sensors were connected to its corresponding charge amplifier and data acquisition system. The data were analyzed using the software *LabVIEW SignalExpress LE*. The in-cylinder pressure is shown in Fig. 5 and the intake and exhaust pressures are shown in Fig. 6. Note that, in this work, the crank angles were chosen with reference to TDC.

Concerning the temperatures, unfortunately, the in-cylinder temperatures can not be measured experimentally because a temperature sensor is not fast enough to accurate capture the in-cylinder temperature along the whole cycle.

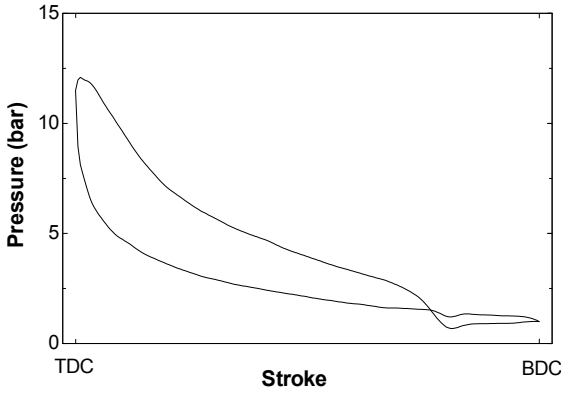

Fig. 5. Evolution of the in-cylinder pressure.

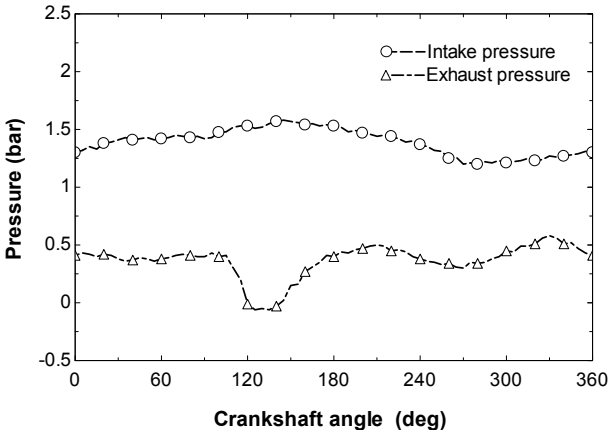

Fig. 6. Evolution of the exhaust and intake pressures.

4.1 Mesh generation

The principle of operation of CFD codes is subdividing the domain into a number of smaller, non-overlapping sub-domains. The result is a grid (or mesh) of cells (or elements). In this work, a grid generation program, Gambit 2.4.6, was used to generate the mesh. In order to implement the movement of the piston, a moving mesh must be used. Figure 7 shows the mesh at several crankshaft angles. The computational domain includes the scavenge ports, exhaust port, cylinder and cylinder head.

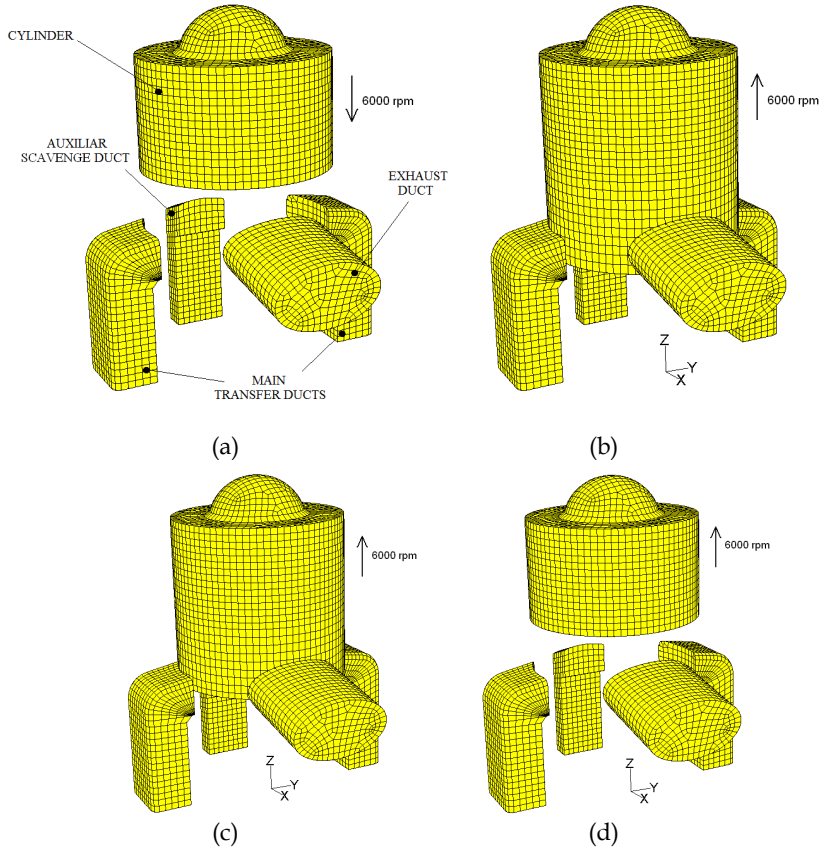

Fig. 7. Computational mesh. (a) 92º crank angle; (b) 190º; (c) 215º; (d) 270º crank angle. Lamas-Galdo *et al.* (2011).

Hexahedral elements provide better accuracy and stability, so a structured hexahedral mesh was adopted. The numerical algorithm implemented automatically updates the mesh after each time step relative to the piston motion using a meshing tool called "dynamic layering", which consists on adding or removing layers of cells adjacent to a moving boundary based on the height of the layer adjacent to the moving surface. The procedure is shown in Fig. 8.

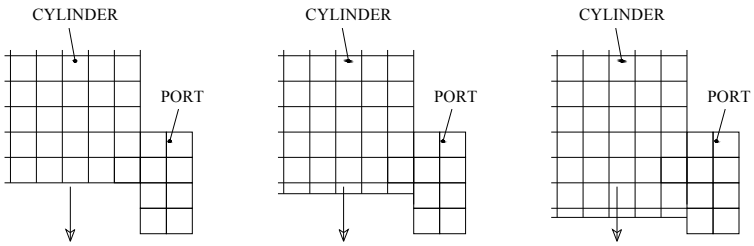

Fig. 8. Layering procedure.

Sometimes it is not possible to employ hexahedral elements in the totality of the control volume. For example, the engine studied in Lamas & Rodríguez (2012), Fig. 1 (b) and Fig. 2 (b), has an exhaust valve in every cylinder. Due to the complex geometry of the valve and duct, tetrahedral elements were employed in that region. Besides, it was necessary to refine the region closed to the valve in order to capture the complex characteristics of the flow. The result is shown in Fig. 9.

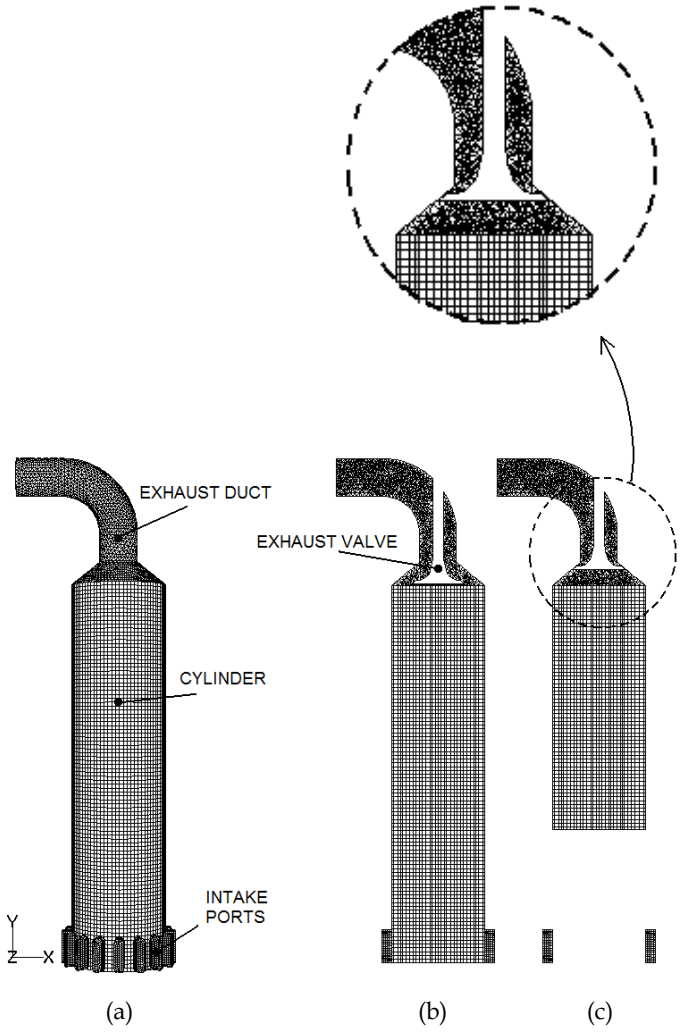

Fig. 9. (a) Tri-dimensional mesh, 180º crankshaft angle. (b) Cross-section mesh, 180º crankshaft angle; (c) Cross-section mesh, 270º crankshaft angle. Lamas & Rodríguez (2012).

It is very important to include the ports and ducts in the computational grid because they notably influence the movement of gases inside the cylinder and therefore the characteristics of the scavenging. For example, in the engine of Fig. 1 (b) and Fig. 2 (b), the intake ports and ducts are inclinated respect to the cylinder axis. Consequently, a swirling motion is promoted by the tangential velocities around the cilinder axis. This phenomena is shown in Fig. 10, which represents the velocity field in a tri-dimensional view, Fig. 10 (a), and in a transversal section at the base of the cylinder, Fig. 10 (b).

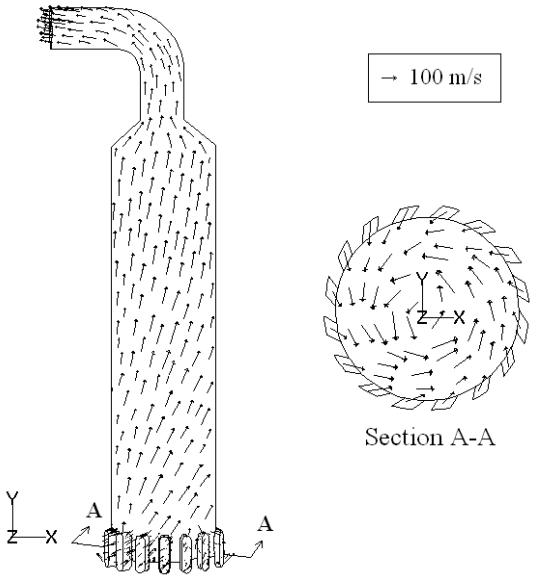

Fig. 10. Velocity field [m/s] for 150º crankshaft angle. (a) Tri-dimensional view. (b) Transversal section A-A, at the base of the cylinder. Lamas & Rodríguez (2012).

Obviously, not all the engines are so sensible to the inlet ports and ducts geometry, but it is recommended to include them in the mesh instead a surface in which a boundary condition is imposed.

4.2 Boundary and initial conditions

All CFD models require initial and boundary conditions. Concerning the pressures, the experimentally values mentioned in the beginning of section 4 were employed as initial and boundary conditions.

As the in-cylinder temperature can not be measured experimentally, the initial temperature must be estimated from an adaptation of the ideal Otto cycle, Fig. 11 (a) and 11 (b). Details of the procedure can be found in most undergraduate textbooks on internal combustion engines or thermodynamics, so they are not repeated here. As can be seen in Fig. 6 (b), the temperature at 90º crankshaft angle is 1027 K.

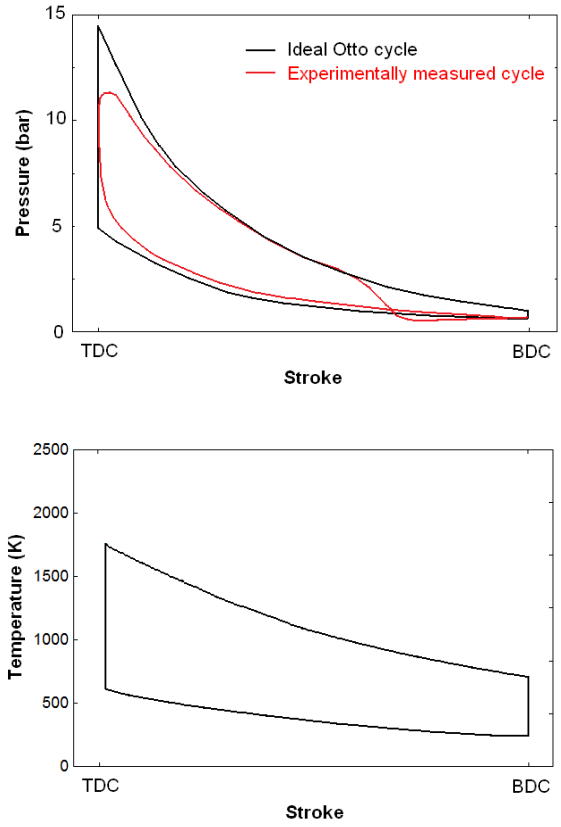

Fig. 11. (a) In-cylinder pressure experimentally measured and obtained from the ideal Otto cycle. (b) In-cylinder temperature obtained from the ideal Otto cycle.

4.3 Resolution of the equations

In this case, the software ANSYS Fluent 6.3 was employed. This is based on the finite volume method. Concerning the time discretization, an implicit method was chosen, with a constant timestep equivalent to 0.1^{o} crankshaft angle. An explicit method could also have been chosen, but implicit methods are unconditionally stables and allow greater time steps. Concerning the pressure-velocity coupling, the PISO algorithm was employed because it is more recommended for transient calculations than the SIMPLE algorithm (Versteeg, 1995). A second order scheme was chosen for discretization of the continuity, momentum, energy and mass fraction equations.

Both the grid and time step sensibility were studied and it was verified that the size of the computational mesh and time increment are adequate to obtain results that are insensitive to further refinement of numerical parameters. In order to ensure this grid independence, several calculations with different mesh sizes and time step sizes were compared.

5. Results

5.1 Pressure field and validation of the code

In order to ensure that the CFD model is accurate enough, numerical results were compared to experimental ones. Particularly, the in-cylinder gauge pressure was validated. For the interval of time studied, from 90º to 270º crankshaft angles, the numerical and experimental results are shown in Fig. 12. Note that an acceptable concordance is obtained between CFD and experimental results.

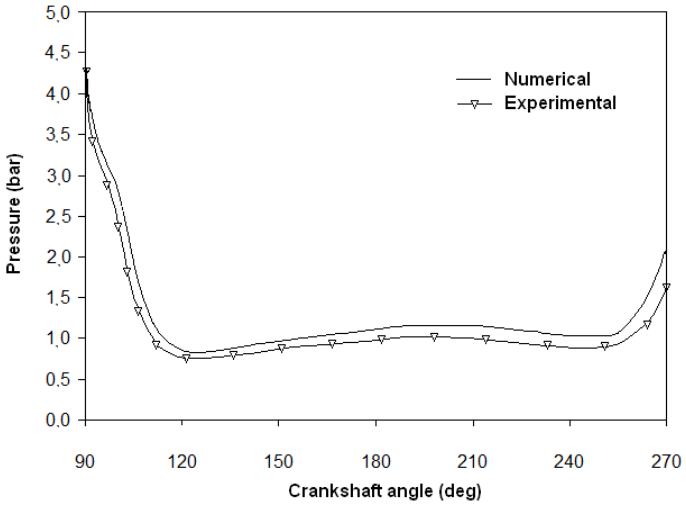

Fig. 12. In-cylinder pressure numerically and experimentally obtained.

Figure 13 shows the gauge pressure field at several crank angles. As can be seen, the initial in-cylinder pressure, Fig. 13 (a), is 4.26 bar. As mentioned before, the intake and exhaust pressures are variable, imposed as boundary conditions at the intake and exhaust ports. At the beginning of the simulation, the pressure descends drastically due to the expansion of the piston (note that the arrows indicate the direction of the piston). When the ports are opened, Fig. 13 (b) and (c), the in-cylinder pressure is slightly superior to the exhaust pressure and slightly inferior to the intake pressure, therefore burnt gasses are expelled through the exhaust port and fresh air enters through the scavenge ports. Finally, when all ports are closed, Fig. 13 (d), the piston is ascending and the gasses are compressed, Fig. 13 (d).

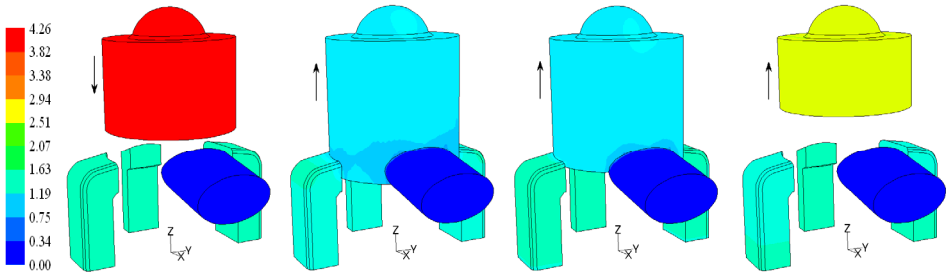

(a) (b) (c) (d)

Fig. 13. Pressure field [bar]. (a) 92º crank angle; (b) 190º crank angle; (c) 215º crank angle; (d) 270º crank angle. Lamas-Galdo *et al.* (2011).

5.2 Mass fraction field

The mass fraction field is shown in Fig. 14. Four positions were represented, 92.5º, 190º, 215º and 270º crank angles. Initially, the cylinder is full of burned gases (blue color), Fig. 14 (a). When the scavenging process begins, the fresh air charge (red color) throws away the burned gases out the cylinder, Fig. 14 (b) and (c). At the end of the process, Fig. 14 (d), the cylinder is full of fresh air charge.

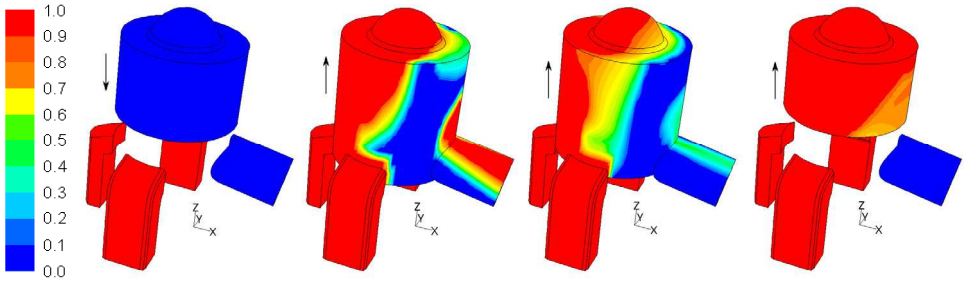

(a) (b) (c) (d)

Fig. 14. Mass fraction field [-]. (a) 92º crank angle; (b) 190º crank angle; (c) 215º crank angle; (d) 270º crank angle. Lamas-Galdo *et al.* (2011).

A very important advantage of CFD codes over experimental setups is that it is very easy to compute the portion of burnt gases which could not be expelled. In this work, it was quantified by means of the scavenging efficiency. This indicates the mass of delivered air that was trapped by comparison with the total mass of air and fresh charge that was retained at exhaust closure, Ec. (13), and its value was 82.5 for the parameters studied.

$$\eta = \frac{mass \;\; of \;\; delivered \;\; air \;\; retained}{mass \;\; of \;\; mixture \;\; in \;\; the \;\; cylinder} \tag{13}$$

The mass fraction field of air of the engine described in Fig. 1 (b) and Fig. 2 (b) is shown in Fig. 15. As can be seen, fresh air (red color) enters through the inlet ports situated at the bottom part of the cylinder and burnt gases (blue color) are expelled through the exhaust valve situated at the top part of the cylinder.

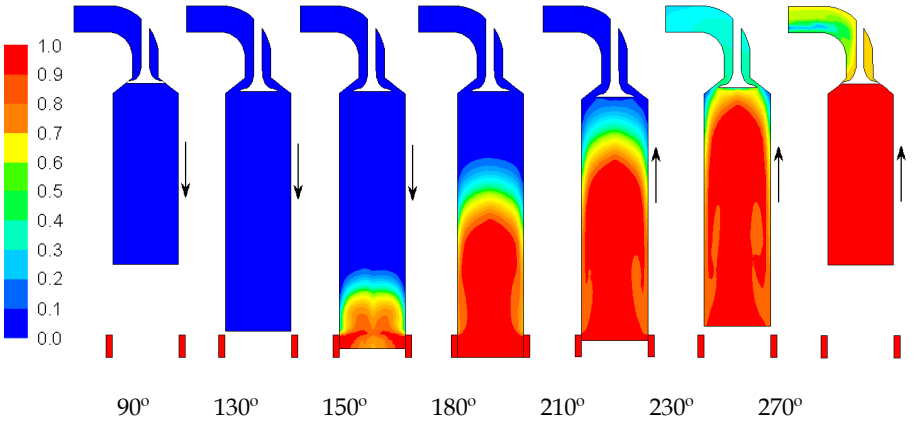

Fig. 15. Mass fraction field of air for several crankshaft positions. Lamas & Rodríguez (2012).

5.3 Velocity field

Fig. 16 shows the velocity field at 92.5º and 190ºcrankshaft angles. It is represented in a cross plane containing the auxiliary transfer port and the exhaust port. As the intake and exhaust ports are opened, fresh charge flows to the cylinder through the scavenge ports and exhaust gasses are expelled thought the exhaust port.

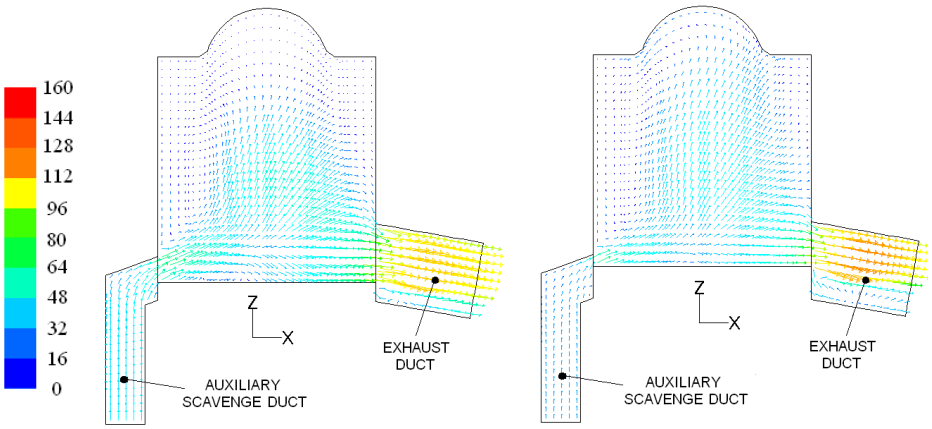

(a) (b)

Fig. 16. Velocity field (m/s). (a) 92º crankshaft angle; (b) 190º crankshaft angle.

5.4 Temperature field

The temperature field at various crank angles is given in Fig 17. As mentioned above, the initial temperature, obtained from the ideal thermodynamic Otto cycle, was imposed as 1027 K, Fig. 17 (a). At the beginning of the simulation, the in-cylinder temperature descends due to the expansion of the piston. When the ports are opened, Fig. 17 (b) and (c), the temperature descends again because fresh air at 300 K enters through the scavenge ports and hot exhaust gases are expelled. At the end of the simulation all the ports are closed and the piston is rising. The compression of the piston makes the temperature increase. Finally, the in-cylinder average temperature at the end of the simulation, Fig. 17 (d), is 677 K.

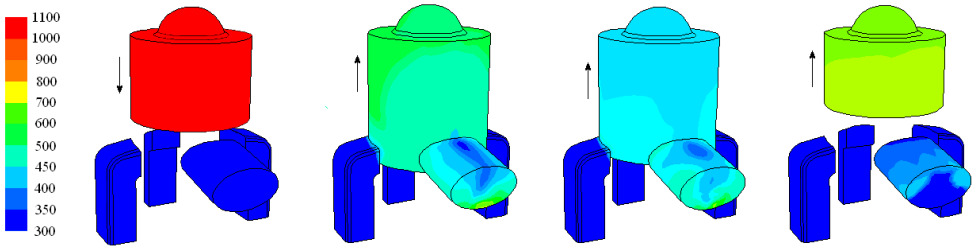

Fig. 17. Temperature field. (a) 92.5º crank angle; (b) 190º crank angle; (c) 215º crank angle; (d) 270º crank angle.

The in-cylinder average temperature and heat transfer from 90º to 270º crankshaft angles is shown in Fig. 18.

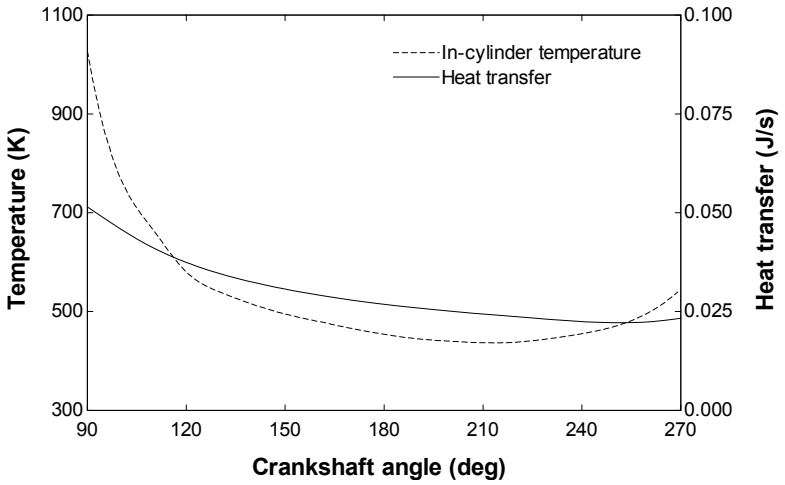

Fig. 18. In-cylinder average temperatura and heat transfer.

6. Conclusions

In the present chapter, a CFD analysis was carried out to study the scavenging process of two-stroke engines. The results were satisfactory compared to experimental data. In general, this study shows that CFD predictions yield reasonably accurate results that allow improving the knowledge of the fluid flow characteristics.

This model is very useful to design the scavenging system of new two-stroke engines. The pressure field is useful for identifying areas where the gas flow is inefficient and should be corrected. The velocity field is useful for locating areas with too high, too low or inadequate orientation velocities. Finally, the mass fraction field is useful for checking the filling of fresh gases into the cylinder and detecting problems of short circuiting and gas drag.

Finally, it is very important to mention the disadvantages of CFD. First of all, a 3D CFD model is very tedious due to the large computational resources. Besides, the moving mesh required to simulate the movement of the piston is too computationally expensive to solve. Other disadvantage is that it must not be applied blindly as it has the capability to produce non-physical results due to erroneous modeling. The process of verification and validation of a CFD model is necessary to ensure the numerical model accurately captures the physical phenomena present. By comparing numerically obtained results with experimental results, confidence in the numerical model is achieved. Once thoroughly validated, a numerical model may be used to accurately predict the effect of design changes and experimentally unobservable phenomena.

7. References

Ahmadi-Befrui, B.; Brandstatter, W.; Kratochwill, H. (1989). Multidimensional calculation of the flow processes in a loop-scavenged two-stroke cycle engine. *SAE Paper 890841*.

Albanesi A., Destefanis C, Zanotti A. (2009) Intake port shape optimization in a four-valve high performance engine. *Mecánica Computacional*. Vol. 28, pp. 1355-1370.

Amsden, A. A.; O´Rourke, P. J.; Butler, T. D.; Meintjes, K. and Fansler, T. D. Comparisons of computed and measured three-dimensional velocity fields in a motored two-stroke engine. SAE Paper 920418, 1992.

Blair G.P. (1996). *Design and Simulation of Two-Stroke Engines*. SAE International. ISBN 978-1-56091-685-7, USA.

Carpenter, M. H.; Ramos, J. I. (1986). Modelling a gasoline-injected two-stroke cycle engine. *SAE Paper 860167*.

Creaven J.P., Kenny K.G., Cunningham G. (2001). A computational and experimental study of the scavenging flow in the transfer duct of a motored two-stroke cycle engine. *Proc Instn Mech Engrs.* Vol.215-D.

Epstein, P. H.; Reitz, R. D. and Foster, D. E. (1991). Computations of two-stroke cylinder and port scavenging. *SAE Paper 919672*.

Fluent 6.3 Documentation, 2006. Fluent Inc.

Hariharan Ramamoorthy, Mahalakshmi N. V., Krishnamoorthy Jeyachandran. (2009). Setting up a comprehensive CFD model of a small two stroke engine for simulation. *International Journal of Applied Engineering Research*. Vol. 4-11.

Hori, H.; Ogawa, T. and Toshihiko, K. (1985). CFD in-cylinder flow simulation of an engine and flow visualization. *SAE Paper 950288*.

Kato S., Nakagawa H., Kawahara Y., Adachi T., Nakashima M. (1991) Numerical analysis of the scavenging flow in a two stroke- cycle gasoline engine. *JSME International Journal*. Vol. 34-3, pp. 385-390.

Laimböck, F. J.; Meist, G. and Grilc, S. (1998). CFD application in compact engine development. *SAE Paper 982016*.

Lamas-Galdo, M.; Rodríguez-Vidal, C.; Rodríguez-García, J.; Fernández-Quintás, M. (2011). Modelo de Mecánica de Fluidos Computacional para el proceso de barrido en un motor Otto de dos tiempos. DYNA Ingeniería e Industria, vol. 86-2, pp. 165-172.

Lamas, M. I.; Rodríguez, C. G. (2012) CFD analysis of the scavenging process in the MAN B&W 7S50MC two-stroke diesel marine engine. Submitted to Journal of Ship Research.

Payri F., Benajes J., Margot X. et al. (2004). CFD modeling of the in-cylinder flow in direct-injection diesel engines. *Computers & Fluids*. Vol.33 p.995-1021.

Pitta S. R., Kuderu R. (2008). A computational fluid dynamics analysis on stratified scavenging system of medium capacity two-stroke internal combustion engines. *Thermal Science*. Vol. 12-1, pp. 33-42.

Raghunathan, B. D. and Kenny, R. G. (1997). CFD simulation and validation of the flow within a motored two-stroke engine. *SAE Paper 970359*.

Rahman M.M., Hamada K.I., Noor M.M. et al. (2010) Heat transfer characteristics of intake port for spark ignition engine: A comparative study. *Journal of applied sciences*. Vol.10-18, pp. 2019-2026.

Sher, E. (1989). An improved gas dynamic model simulating the scavenging process in a two-stroke cycle engine. *SAE Paper 800037*.

Sweeny, M. E. G.; Kenny, R. G.; Swann, G. B. G. and Blair, G. P. (1985). Computational fluid dynamics applied to two-stroke engine scavenging. *SAE Paper 851519*.

Yu, L.; Campbell, T. and Pollock, W. (1997). A simulation model for direct-fuel-injection of two-stroke gasoline engines. *SAE Paper 970367*.

Zahn, W.; Rosskamp, H.; Raffenberg, M. and Klimmek, A. (2000). Analysis of a stratified charging concept for high-performance two-stroke engine. *SAE Paper 2000-01-0900*.

Zancanaro F.V., Vielmo H.A. (2010) Numerical analysis of the fluid flow in a high swirled diesel engine. *Proceedings of the 7th International Conference on Heat Transfer, Fluid Mechanics and Thermodynamics*. Antalya-Turkey, 19-21 July 2010, pp. 387-392.

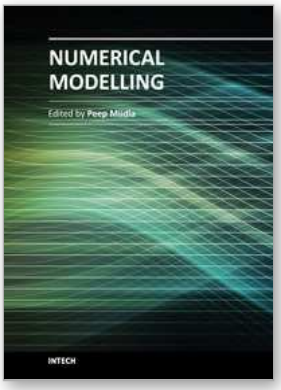

Numerical Modelling
Edited by Dr. Peep Miidla

ISBN 978-953-51-0219-9
Hard cover, 398 pages
Publisher InTech
Published online 23, March, 2012
Published in print edition March, 2012

This book demonstrates applications and case studies performed by experts for professionals and students in the field of technology, engineering, materials, decision making management and other industries in which mathematical modelling plays a role. Each chapter discusses an example and these are ranging from well-known standards to novelty applications. Models are developed and analysed in details, authors carefully consider the procedure for constructing a mathematical replacement of phenomenon under consideration. For most of the cases this leads to the partial differential equations, for the solution of which numerical methods are necessary to use. The term Model is mainly understood as an ensemble of equations which describe the variables and interrelations of a physical system or process. Developments in computer technology and related software have provided numerous tools of increasing power for specialists in mathematical modelling. One finds a variety of these used to obtain the numerical results of the book.

InTech Europe
University Campus STeP Ri
Slavka Krautzeka 83/A
51000 Rijeka, Croatia
Phone: +385 (51) 770 447
Fax: +385 (51) 686 166
www.intechopen.com

InTech China
Unit 405, Office Block, Hotel Equatorial Shanghai
No.65, Yan An Road (West), Shanghai, 200040, China
中国上海市延安西路65号上海国际贵都大饭店办公楼405单元
Phone: +86-21-62489820
Fax: +86-21-62489821